

Electromagnetic Formation Flight

Progress Report: May 2003

Submitted to: Lt. Col. John Comtois
Technical Scientific Officer
National Reconnaissance Office

Contract Number: NRO-000-02-C0387-CLIN0001

MIT WBS Element: 6893087

Submitted by: Prof. David W. Miller

Space Systems Laboratory
Massachusetts Institute of Technology

OVERVIEW

Description of the Effort

The Massachusetts Institute of Technology Space Systems Lab (MIT SSL) and the Lockheed Martin Advanced Technology Center (ATC) are collaborating to explore the potential for an Electro-Magnetic Formation Flight (EMFF) system applicable to Earth-orbiting satellites flying in close formation.

Progress Overview

At MIT, work on EMFF has been pursued on two fronts: the MIT conceive, design, implement and operate (CDIO) class, and the MIT SSL research group.

This report summarizes recent progress made in the MIT CDIO class with regards to system dynamic modeling, linear control design, and closed-loop control implementation on the electromagnetic formation flight testbed being designed and built in the class.

First the testbed control requirements and experimental testing plan (“test cases”) are presented, and the linearized dynamic model of the testbed system is discussed. Then the linear control design methodology is reviewed, and the resulting control gains specific to each test case are presented. Finally, successful closed-loop dynamic results are presented for test cases 1a and 1b.

A Control Algorithm Development

A.1 Control Requirements

Electromagnets and reaction wheels are used to provide the forces and torques necessary to control position and attitude of the vehicles. The interaction between electromagnets of different vehicles can be controlled to either attract or repel the vehicles. The reaction wheels can rotate either clockwise or counterclockwise, providing control to either accelerate or decelerate the vehicles rotationally. Varying the current through the magnets and changing the speed of the wheels control the actuators. Controlling these accurately allows for maneuvering the vehicles and disturbance rejection.

The responsibility of the control team was to build a robust controller for the project that will command maneuvers and provide disturbance rejection. The controller is located on the avionics computer, and processes metrology inputs in order to calculate the necessary commands to send to the actuators. This is depicted in the block diagram in Figure A.1-A.

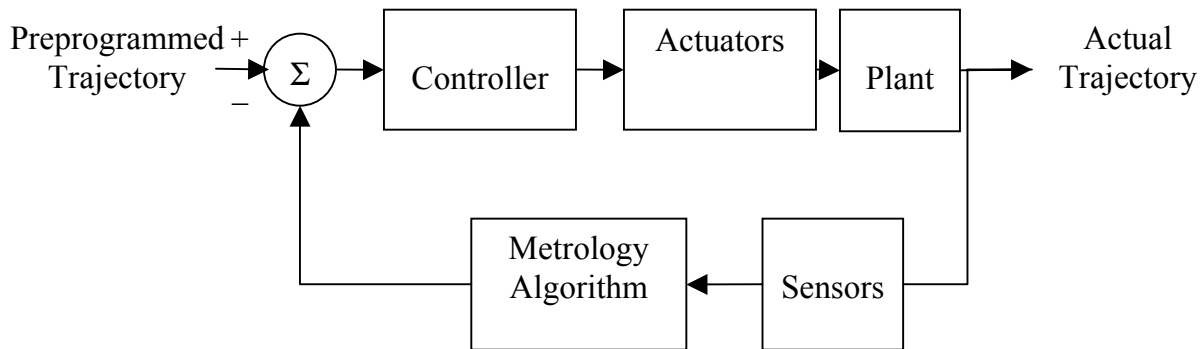


Figure A.1-A: Block Diagram of Controller

The control team designed controllers to meet the following requirements, derived from the requirements document.

1. Exhibit control in two modes
 - a. Spin-up/spin-down
 - b. Steady state
2. Build a robust controller for two types of maneuvering
 - a. Trajectory following
 - b. Disturbance rejection
3. Maximum allowable error in separation distance is 15 centimeters for a separation distance of 2 meters between vehicles

4. Maximum allowable error in angular position is 5 degrees for each vehicle's orientation
5. Rotation rate in steady state must be one revolution per minute

The first requirement specifies the modes in which the test-bed operates. This is derived from the test case in which two vehicles are at rest, spin-up to steady state, and then spin-down to rest. Spin-up consists of controlling two vehicles initially at rest and positioned so that the electromagnet of the first vehicle is perpendicular to that of the second, as shown in Figure A.1-B. When the electromagnets are turned on, the vehicles rotate and shear in the directions of the arrows. By controlling the electromagnets and reaction wheels, thereby applying appropriate forces and torques on the vehicles, the vehicles will follow the trajectory specified in Figure A.2-C, where the arrows point to the “north pole” of the magnets.

This path will guide the vehicles to the steady state configuration, in which the electromagnets are aligned along a common axis, as show Figure A.1-D, and spinning at a constant rate, Ω , about their common center. Finally, spin-down follows the same trajectory as spin-up but in reverse. In spin-down, as the magnets rotate in the opposite direction relative to the radial line between the electromagnets to align perpendicularly, the test-bed comes to rest. A controller has been designed for spin-up, but has not yet been tested.

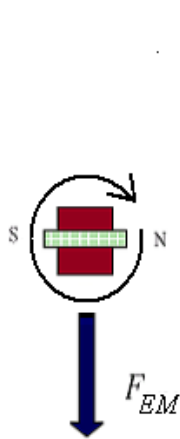


Figure A.1-B: Spin-up Mode Trajectory

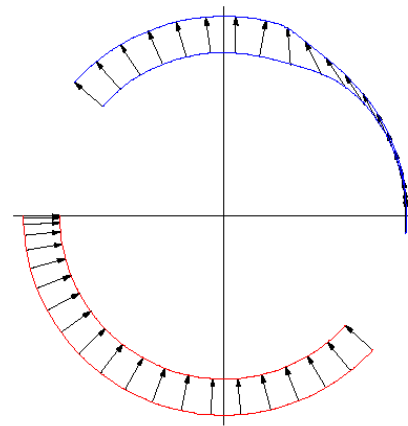


Figure A.1-C: Spin-up

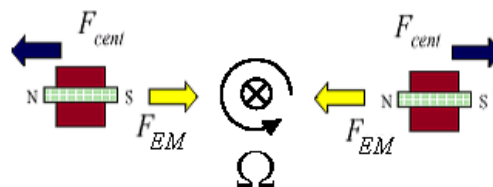


Figure A.1-D: Steady State Spin Mode

To achieve a robust controller implies two responsibilities. The test-bed must both reject disturbances as well as have the control authority to reposition the vehicles. Rejecting disturbances implies both maintaining desired positions and desired angular rates, whether finite or zero in the presence of external disturbances. The controller was designed to demonstrate these capabilities in both the spin-up/spin-down as well as steady-state modes. Repositioning of the vehicles was to be used during the spin-up and spin-down maneuvers by following a user-supplied trajectory.

Requirements three and four set the displacement and angular accuracies required for a successful controller. When the controller determines the desired displacement and angular position for each vehicle, they must reach these states with a set accuracy for the controller to work. These accuracies were derived from the accuracy of our system model. The model was obtained by adding a perturbation to the non-linear system dynamics and linearizing the equations of motion. In this process, higher order terms were neglected.

To see when these higher order terms become negligible, further analysis was done by comparing the linearized model with the full non-linear model for different size perturbations. The electromagnetic forces on each vehicle due to the electromagnetic interaction between the vehicles were calculated in the x direction for each model. This calculation was done by creating a force balance, as shown in Figure A.1-D. Holding all terms except separation distance constant, the results are as follows:

$$F_{x,non-linear} = \frac{1}{(r + \delta r)^4} \left(-\frac{3}{2\pi} \mu_0 \mu_{A1} \mu_{B1} - \frac{3}{4\pi} \mu_0 \mu_{A2} \mu_{B2} \right) \quad \text{Equation A.1-1}$$

$$F_{x,linear} = \frac{1}{r^4} \left(1 - 4 \frac{\delta r}{r} \right) \left(-\frac{3}{2\pi} \mu_0 \mu_{A1} \mu_{B1} - \frac{3}{4\pi} \mu_0 \mu_{A2} \mu_{B2} \right) \quad \text{Equation A.1-2}$$

where \mathbf{r} is the separation distance, $\delta \mathbf{r}$ is a perturbation added to the separation distance, and the $\boldsymbol{\mu}$ terms are the magnetic moments for the different coils. The ratio between the linearized forces and non-linear forces is defined as α , where

$$\alpha = \frac{non-linear}{linearized} = \frac{1 / \left(1 + \frac{\delta r}{r} \right)^4}{1 - 4 \frac{\delta r}{r}} \quad \text{Equation A.1-3}$$

Substituting two meters for the separation distance \mathbf{r} provides Figure A.1-E for α as a function of perturbation size, $\delta \mathbf{r}$.

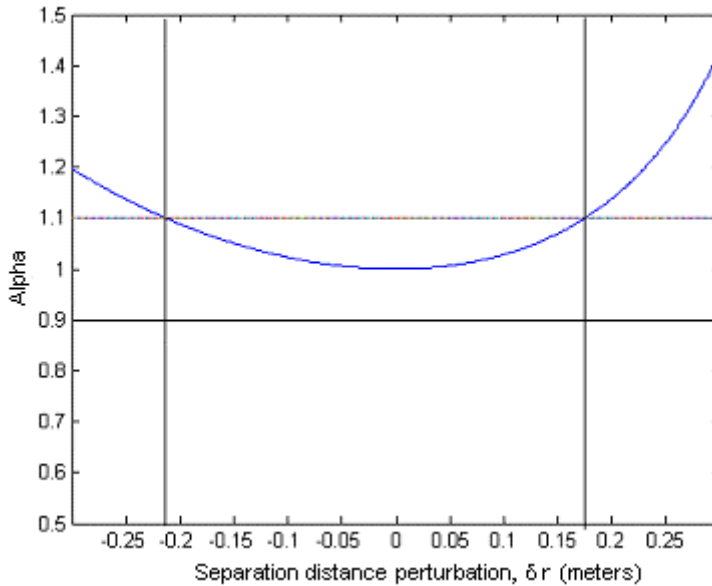


Figure A.1-E: Alpha as a Function of Separation Distance Perturbation

At alpha equal to one, there is no difference between the linear model and actual model. It was decided that a 10% difference between the models would still produce a functional controller. This difference is shown in the graph by the horizontal lines at alpha equal to 1.1 and 0.9. Therefore, there is less than a 10% difference between models when the distance error is between -0.22m and 0.17m, as shown by the vertical lines. To be conservative, the maximum separation distance error was set at ± 0.15 m, guaranteeing less than a 10% difference between the linearized model used to calculate the control and the full non-linear system.

A similar approach of analyzing the linearized model was used to determine the maximum allowable angle error. The forces were examined again holding all terms constant except the angle of the magnet with respect to the other magnet. The Mathematica code was used to try different size angular perturbations and compare the output forces from both the linear and non-linear models. A perturbation of 5 degrees creates a difference of less than 10% between the two models, and therefore is used as the limit for accuracy.

Finally, there was a requirement setting the rotation rate in steady state. It must be at least one revolution per minute. This was to limit the duration of testing due to a limited CO₂ supply and battery life, as well as to allow the controller to dominate over frictional forces and slopes in the flat floor. At slower speeds, the frictional forces may become significant, creating errors in the system models that do not account for friction. Therefore, it was important to maintain a speed at which friction is not a factor so the system model remains accurate and the controllers are effective.

A.2 Test Cases

There were several steps to designing the controller. The first was to break down the requirements into smaller test cases. For each test case, the system was modeled, a controller was designed and then coded onto the processor and integrated into the final system. These controllers were then tested and refined. The test cases were defined as follows:

1. One vehicle (only reaction wheel control)
 - 1a. Disturbance rejection
 - 1b. Trajectory following
2. Two vehicles (reaction wheel and electromagnet control)
 - 2a. One vehicle fixed, disturbance rejection
 - 2b. One vehicle fixed, trajectory following and slewing
 - 2c. Both vehicles free, disturbance rejection
 - 2d. Both vehicles free, trajectory following and slewing
 - 2e. Spin-up to steady state, then spin-down.

The first set of test cases uses only one vehicle, so there is no electromagnet control, since this requires a second vehicle with an electromagnet. In Test Case 1a, disturbance rejection was demonstrated by maintaining both a zero rotation rate and finite rotation rate by commanding the reaction wheel. In Test Case 1b, trajectory following was demonstrated by rotating the vehicle to a commanded angle.

The second set of test cases adds another vehicle, as well as the use of the electromagnet actuators. In the first two cases, one vehicle is fixed so it cannot move. The other vehicle will demonstrate disturbance rejection as well as trajectory following by moving to commanded separation distances as well as commanded angular positions. In the next two cases, both vehicles are free. Therefore both vehicles can be disturbed as well as commanded to new positions. Finally, a two vehicle spin-up, steady-state spin, and spin-down maneuver must be performed.

Originally, a Test Case 3 was designed in which three vehicles would have been controlled. A third vehicle was never built, so the third test case was never tested. Controllers have been designed for this test case, however, and are therefore included as a reference for future work. Test Case 3 was defined as:

3. Three vehicles (reaction wheel and electromagnet control)
 - 3a. Central vehicle fixed, disturbance rejection
 - 3b. Central vehicle fixed, trajectory following and slewing
 - 3c. All vehicles free, disturbance rejection
 - 3d. All vehicles free, trajectory following and slewing
 - 3e. Spin-up to steady state, then spin-down.

The third test case is similar to Test Case 2, with the addition of one more vehicle. In the first two parts of the test, the middle vehicle is fixed and the other two must demonstrate disturbance rejection and slewing. Then all the vehicles are freed. In the final test case, three vehicles must perform the full spin-up, steady state, spin-down maneuver.

A.3 System Model

The design of the controller begins with a model of the system. Because each vehicle has inputs from both an electromagnet and a reaction wheel, and there are different states that need to be controlled, a state space model of the system is used to model the system. Since the system has no inertial reference, a coordinate system will be fixed on a specified body. In the diagram below (Figure A.3-A), the coordinate system is fixed on Vehicle A. Here, the states of interest are the distance to the other vehicle (r_{AB}), the angle to the other vehicle from a reference point (θ_{AB}), the angle rotated by each vehicle about its own center of mass (α_A , α_B) from the radial line between vehicles, the rates of these states, as well as the angular rate of the entire system (Ω).

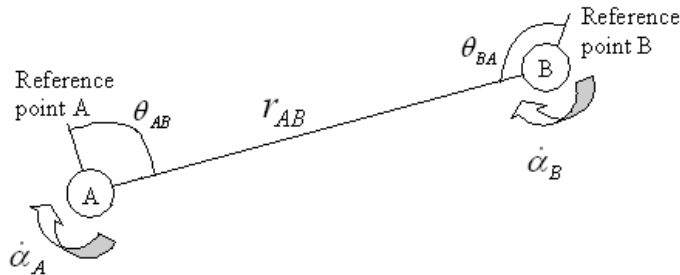


Figure A.3-A: Definition of States

The states are organized into a vector \mathbf{x} :

$$\mathbf{x} = \begin{bmatrix} \mathbf{r} \\ \boldsymbol{\theta} \\ \boldsymbol{\alpha} \\ \dot{\mathbf{r}} \\ \dot{\boldsymbol{\theta}} \\ \dot{\boldsymbol{\alpha}} \\ \Omega \end{bmatrix} \quad \text{Equation A.3-1}$$

where the first six states are vectors representing states for each vehicle. These states are named the Master State Array (MSA) and will be computed by metrology, transmitted by communications, and entered as inputs to the controller.

By linearizing the equations of motion, system models were developed for each test case of the form:

$$\dot{\mathbf{x}} = \mathbf{A}\mathbf{x} + \mathbf{B}\mathbf{u} \quad \text{Equation A.3-2}$$

$$\mathbf{y} = \mathbf{C}\mathbf{x} + \mathbf{D}\mathbf{u} \quad \text{Equation A.3-3}$$

where \mathbf{x} are the states, \mathbf{u} are the inputs, and \mathbf{y} are the measurements. The \mathbf{A} and \mathbf{B} matrices were determined for each test case with variable system parameters. Estimates were made and used to design the preliminary controllers, and were refined when new system information was known.

For Test Case 1, the desired states were defined as

$$x = \begin{bmatrix} \theta \\ \dot{\theta} \end{bmatrix} \quad \text{Equation A.3-4}$$

where θ is the angular position of the vehicle relative to its initial position, and $\dot{\theta}$ is its angular rate. The driving dynamics of the system are the torque produced by the reaction wheel, τ , and the resultant torque on the vehicle, $I\ddot{\theta}$. The vehicle was approximated as a cylinder to determine the inertia, I . The output of the system is the gyro reading, or $\dot{\theta}$. Putting these into state space form produces:

$$\dot{x} = \begin{bmatrix} 0 & 1 \\ 0 & 0 \end{bmatrix} x + \begin{bmatrix} 0 \\ 1/I \end{bmatrix} \tau \quad \text{Equation A.3-5}$$

$$y = [0 \quad 1]x \quad \text{Equation A.3-6}$$

For Test Case 2 the model is a bit more complex, thus we used Mathematica to compute it. Our model of the system uses Figure A.3-B as a reference for the variables in the Mathematica script.

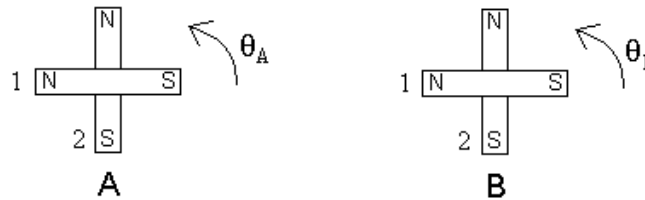


Figure A.3-B: Model of system for test case 2

For the purpose of this paper we will only analyze test case 2. The analysis for test case 3 is done in the same way. Figure A.3-B shows two vehicles, vehicles A and B, each with two electromagnets, magnets 1 and 2. We will use body coordinates fixed on vehicle B, therefore vehicle B will not translate. The angular position of vehicle A, θ_A , will be measured from the axis connecting vehicle A and vehicle B. We start with the equations of motion where the forces and torques, T and F , are for each of the interactions between the coils – A1, A2, B1, B2 – in the direction indicated, x or y:

$$m\ddot{x}_A = F_{A1/B1,x} + F_{A1/B2,x} + F_{A2/B1,x} + F_{A2/B2,x} \quad \text{Equation A.3-7}$$

$$m\ddot{y}_A = F_{A1/B1,y} + F_{A1/B2,y} + F_{A2/B1,y} + F_{A2/B2,y} \quad \text{Equation A.3-8}$$

$$I_{A,Z} \ddot{\theta}_A = T_{A1/B1} + T_{A1/B2} + T_{A2/B1} + T_{A2/B2} + T_{RW,A} \quad \text{Equation A.3-9}$$

$$I_{B,Z} \ddot{\theta}_B = T_{B1/A1} + T_{B1/A2} + T_{B2/A1} + T_{B2/A2} + T_{RW,B} \quad \text{Equation A.3-10}$$

By linearizing these equations and dropping the higher order terms, one can construct the state space model of the system. The model for tests 2a and 2b, in the form $\dot{\mathbf{x}} = \mathbf{Ax} + \mathbf{Bu}$, is shown in Figure A.3-C:

$$\dot{\mathbf{x}} = \begin{bmatrix} 0 & 0 & 0 & 1 & 0 & 0 \\ 0 & 0 & 0 & 0 & 1 & 0 \\ 0 & 0 & 0 & 0 & 0 & 1 \\ 0 & 0 & 0 & 0 & 0 & 0 \\ 0 & 0 & 0 & 0 & 0 & 0 \\ 0 & 0 & 0 & 0 & 0 & 0 \end{bmatrix} \begin{bmatrix} x_A \\ y_A \\ \theta_A \\ \dot{x}_A \\ \dot{y}_A \\ \dot{\theta}_A \end{bmatrix} + \begin{bmatrix} 0 & 0 & 0 \\ 0 & 0 & 0 \\ 0 & 0 & 0 \\ \frac{-15\mu_0\mu_{B1}}{2\pi n_A r^4} & \frac{15\mu_0\mu_{B2}}{4\pi n_A r^4} & 0 \\ \frac{15\mu_0\mu_{B2}}{4\pi n_A r^4} & \frac{15\mu_0\mu_{B1}}{4\pi n_A r^4} & 0 \\ \frac{-\mu_0\mu_{B2}}{\pi I_{A,Z} r^3} & \frac{-2\mu_0\mu_{B1}}{\pi I_{A,Z} r^3} & \frac{1}{I_{A,Z}} \end{bmatrix} \begin{bmatrix} \mu_{A1} \\ \mu_{A2} \\ T_{RW,A} \end{bmatrix}$$

Figure A.3-C: State space equation for tests 2a and 2b

And the model for tests 2c, 2d, and 2e is given in Figure A.3-D:

$$\dot{\mathbf{x}} = \begin{bmatrix} 0 & 0 & 0 & 0 & 1 & 0 & 0 & 0 \\ 0 & 0 & 0 & 0 & 0 & 1 & 0 & 0 \\ 0 & 0 & 0 & 0 & 0 & 0 & 1 & 0 \\ 0 & 0 & 0 & 0 & 0 & 0 & 0 & 1 \\ 0 & 0 & 0 & 0 & 0 & 0 & 0 & 0 \\ 0 & 0 & 0 & 0 & 0 & 0 & 0 & 0 \\ 0 & 0 & 0 & 0 & 0 & 0 & 0 & 0 \\ 0 & 0 & 0 & 0 & 0 & 0 & 0 & 0 \end{bmatrix} \begin{bmatrix} x_A \\ y_A \\ \theta_A \\ \theta_B \\ \dot{x}_A \\ \dot{y}_A \\ \dot{\theta}_A \\ \dot{\theta}_B \end{bmatrix} + \begin{bmatrix} 0 & 0 & 0 & 0 \\ 0 & 0 & 0 & 0 \\ 0 & 0 & 0 & 0 \\ \frac{-15\mu_0\mu_{B1}}{2\pi n_A r^4} & \frac{15\mu_0\mu_{B2}}{4\pi n_A r^4} & 0 & 0 \\ \frac{15\mu_0\mu_{B2}}{4\pi n_A r^4} & \frac{15\mu_0\mu_{B1}}{4\pi n_A r^4} & 0 & 0 \\ \frac{-\mu_0\mu_{B2}}{\pi I_{A,Z} r^3} & \frac{-2\mu_0\mu_{B1}}{\pi I_{A,Z} r^3} & \frac{1}{I_{A,Z}} & 0 \\ \frac{-2\mu_0\mu_{B2}}{\pi I_{B,Z} r^3} & \frac{-\mu_0\mu_{B1}}{\pi I_{B,Z} r^3} & 0 & \frac{1}{I_{B,Z}} \end{bmatrix} \begin{bmatrix} \mu_{A1} \\ \mu_{A2} \\ T_{RW,A} \\ T_{RW,B} \end{bmatrix}$$

Figure A.3-D: State space equation for tests 2a, 2b, and 2c

where $r = \sqrt{x_A^2 + y_A^2}$.

The key difference between these models is the fact that for tests 2c, 2d, and 2e vehicle B is not fixed, allowing for the use of its reaction wheel for control. The state space models for test case 3 are similarly found. The state space models above were computed using

specific values for the field strengths of the magnets on the fixed vehicle. The model will have to be recomputed to get the correct gains for different test case setups.

A.4 Reaction Wheel Motor Model

The reaction wheel assembly, which controls the attitude of the vehicle, is powered by a single motor mounted in the center of the vehicle. The behavior of the motor is essential to overall vehicle dynamics. The motor behavior was modeled to extract constants needed for the controller. The controller used initially for the motor used proportional control. The proportional controller did not provide precise enough control, so a first-order model was derived, beginning with the relationships:

$$(T + b\omega) \frac{R_a}{k_t} + k_e \omega = V \quad \text{Equation A.4-1}$$

$$T = k_t i \quad \text{Equation A.4-2}$$

where T is motor torque, b is a frictional constant, ω is the rate at which the motor shaft spins, R_a is the armature resistance of the motor, k_t and k_e are torque constants, and V is the voltage required by the motor.

If you assume that the current supplied to the motor remains constant, only the frictional constant needs to be found. The frictional constant, b was found experimentally. The wheel was mounted on the motor and spun up to maximum speed. The motor was then turned off and measurements of ω were taken at regular intervals until the wheel came to a complete stop. The rate of rotation measurements were taken with the tachometer. Test data is shown in Table A.4-1 below. The time shown is the time since the motor was turned off.

Table A.4-1 Reaction wheel motor data

Time (s)	Trial 1 - ω (Hz)	Trial 2 - ω (Hz)
0	208	185
5	185	161
10	172	156
15	155	135
20	138	125
25	122	111
30	106	96
35	102	87
40	87	75
45	75	64
50	67	54
55	57	43
60	45	34
65	34	26
70	27	19
75	20	12
80	12	6

The frictional constant b was derived from the relationship:

$$I_{wheel} \ddot{\Theta} + b \dot{\Theta} = k_t i \quad \text{Equation A.4-3}$$

giving a value of b :

$$b = -0.000379 \frac{kgm^2}{s} \quad \text{Equation A.4-4}$$

We also tried to make a better model by taking out our constant current assumption. We abandoned this as soon as the first order model was found to work but I will include the work here anyway.

Integration of Equation A.5-3 gives:

$$i(t) = ce^{-\frac{R_a t}{L_a}} + \frac{V}{R_a} \quad \text{Equation A.4-5}$$

Taking data on the motor and solving Equation A.5-4 graphically for inductance gives:

$$L_a = 1.33 \times 10^{-5} \text{ H} \quad \text{Equation A.4-6}$$

A.5 Controller Design

The technique of control design used for the test-bed was the linear quadratic regulator, providing an optimal controller. The LQR approach minimizes the cost equation:

$$J = \int (x^T R_{xx} x + u^T R_{uu} u) dt \quad \text{Equation A.5-1}$$

where \mathbf{J} is the cost, \mathbf{x} is the state, \mathbf{u} is the control input, R_{xx} is the cost associated with state, and R_{uu} is the cost associated with the control. When importance is placed on state accuracy, and the amount of control, or current to the actuators, is less important, R_{xx} is weighted high. When minimizing the amount of control used is more important than the accuracy of the state, R_{uu} is weighted high. To find the minimal cost \mathbf{J} , the following equation must be solved for \mathbf{P} :

$$0 = R_{xx} + PA + A^T P - PB R_{uu}^{-1} B^T P \quad \text{Equation A.5-2}$$

where \mathbf{A} and \mathbf{B} are the same matrices found in modeling the system. The value of \mathbf{P} can be used to find the optimal gains, \mathbf{F} , for the system, where:

$$F = R_{uu}^{-1} B^T P \quad \text{Equation A.5-3}$$

The optimal control is then,

$$u = -Fx \quad \text{Equation A.5-4}$$

Substituting into Equation A.4-2, the closed loop A matrix can be determined, where

$$A_{CL} = A - BF \quad \text{Equation A.5-5}$$

This was calculated in Matlab using the LQR command. After determining the A and B matrices, as well as the weightings for R_{xx} and R_{uu} , these values are entered as parameters for the LQR function.

$$[F, S, E] = lqr(A, B, R_{xx}, R_{uu}) \quad \text{Equation A.5-6}$$

A.5.1 Test Case 1a

The angular rate of the vehicle was controlled through a simple feedback gain, using a rate gyro for feedback. This gain was determined using LQR techniques.

For this disturbance rejection case, the weightings were set to

$$R_{xx} = \begin{bmatrix} 10^{-5} & 0 \\ 0 & 1 \end{bmatrix} \quad R_{uu} = \frac{1}{4} \quad \text{Equation A.5-7}$$

In the actual code, the matrix entries of zero were replaced with finite numbers due to the fact that singularities were being created in the LQR function. The higher weighting on $\dot{\theta}$ in \mathbf{R}_{xx} compared to the \mathbf{R}_{uu} weighting indicates that it is more important to have an accurate $\dot{\theta}$ than it is to conserve control energy. The weightings along the diagonal of \mathbf{R}_{xx} place more importance on the second state, $\dot{\theta}$, than on the first state. This is because in disturbance rejection, the actual position is not controlled. The rate of change of position is driven to zero, and therefore the rate is weighted more heavily. These weightings were used in Matlab with the \mathbf{A} and \mathbf{B} matrices from Equation A.4-5. For an inertia of $1 \text{ kg}\cdot\text{m}^2$, the optimal gains are:

$$F = [0.0063 \quad 2] \quad \text{Equation A.5-8}$$

This inertia estimate includes the weight of the LN2. If the test was run without the coils filled, the inertia estimate lowers to $0.9 \text{ kg}\cdot\text{m}^2$ but the gains remain unaffected at

$$F = [0.0063 \quad 2] \quad \text{Equation A.5-9}$$

The controller was tested on a vehicle by giving manual disturbances. The vehicle successfully returned to a zero position, as shown in Figure A.5-A.

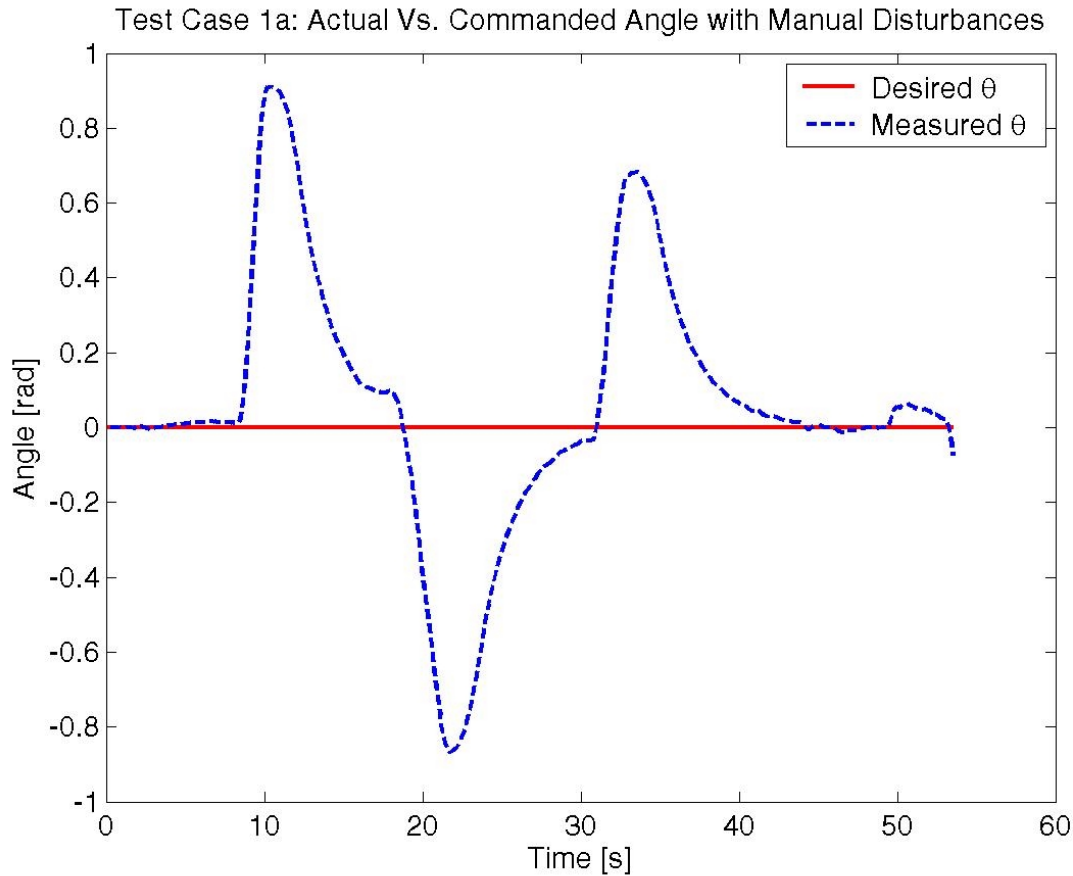


Figure A.5-A: Vehicle response to manual disturbances

A.5.2 Test Case 1b

A controller was designed for Test Case 1b, a tracking problem. The same system model was used for this problem. However, different costs were assigned, as shown below:

$$R_{xx} = \begin{bmatrix} 1 & 0 \\ 0 & 10^{-4} \end{bmatrix} \quad R_{uu} = \frac{1}{4} \quad \text{Equation A.5-10}$$

In this case, the weightings along the diagonal of \mathbf{R}_{xx} place more importance on the first state, θ . In a tracking problem, the specific position is more important than the rate of change of the position. The accuracy of the state is still more important than the amount of control used, as shown in the difference in magnitude between \mathbf{R}_{xx} and \mathbf{R}_{uu} . The new gains for were found to be:

$$F = [2.000 \quad 1.898] \quad I = 0.9 \text{ kg}\cdot\text{m}^2 \quad \text{Equation A.5-11}$$

$$F = [2.000 \quad 2.001] \quad I = 1 \text{ kg}\cdot\text{m}^2 \quad \text{Equation A.5-12}$$

Comparing these gains to those calculated for Test Case 1a shows how the relative gain on θ increases in the slewing case of 1b, reflecting the shift in importance of position.

This controller was tested by providing inputs, commanding the vehicle to rotate to different angles. There was a fairly significant time lag, which can be improved by tweaking the gains. The results of this test are shown in Figure A.5-B.

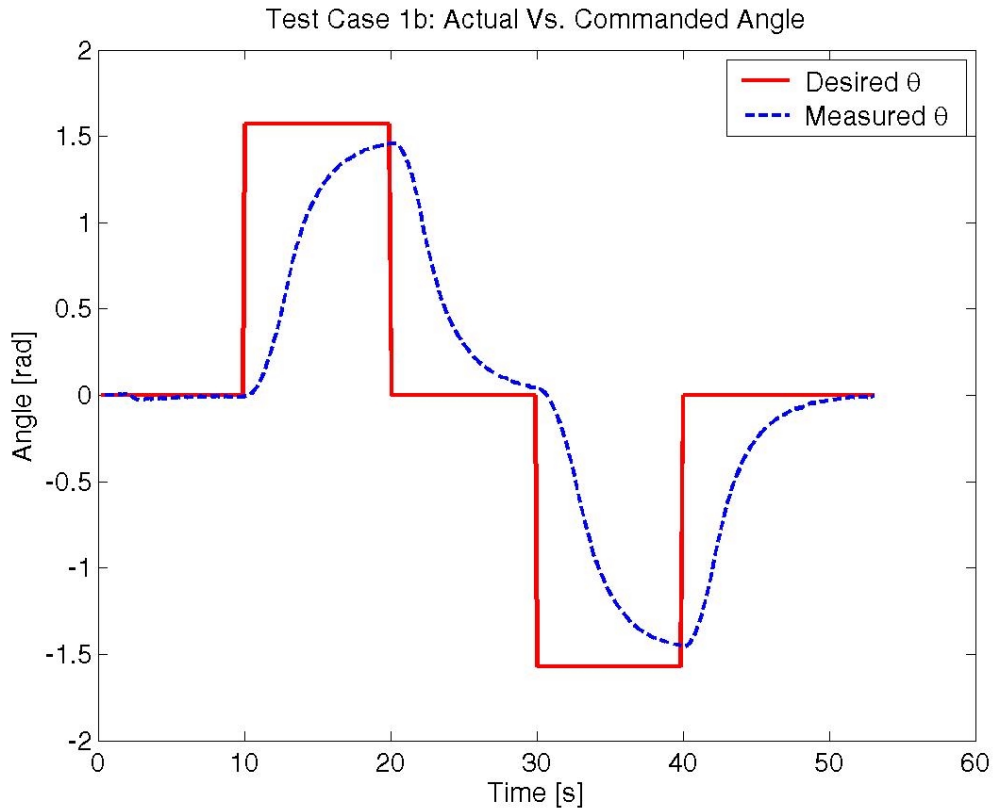


Figure A.5-B: Vehicle response to commanded inputs

A.5.3 Test Cases 2 and 3

Optimal gains were determined for Test Cases 2 and 3 in the same manner using the system models described above. Weightings were chosen in a similar fashion to the ones chosen for test case one, with the rates weighted more for disturbance rejection, and the positions weighted more for trajectory following. In all cases the states were weighted more heavily than the control. Sample gains for Test Case 2a are shown below in Table A.5-1. A vehicle mass of 15 kg was used, with an inertia of $1 \text{ kg}\cdot\text{m}^2$ for both vehicles.

Table A.5-1: Optimal Gains for Test Case 2a

x_A	y_A	θ_A	\dot{x}_A	\dot{y}_A	$\dot{\theta}_A$	
-0.0063	0.0004	-0.0000	-23.9293	1.9237	-0.0000	μ_{A1}
0.0004	0.0063	-0.0000	1.9237	33.7807	-0.0003	μ_{A2}
0.0000	0.0000	0.0089	0.0001	0.0060	2.8316	$\tau_{RW,A}$

There is a gain associated with each state and input pair. Only the states and inputs of vehicle **A** are used in Test Case 2a because the other vehicle is fixed. The states of interest are listed across the top row with the subscript **A** referring to vehicle **A**, and the inputs are listed in the last column. Here, **x** and **y** are the rectangular decomposition of the position **r** described in Table A.5-1 above. The inputs μ_{A1} and μ_{A2} refer to the current needed to drive the two electromagnet coils per vehicle, and $\tau_{RW,A}$ is the torque required from the reaction wheel. Because Test Case 2a is a disturbance rejection problem, the gains associated with the rates are higher.

The rest of the gains are given in section A.9. For Test Case 3, a vehicle mass of 15 kg was used and an inertia of 1.0547 kg*m² was used. There are no optimal gains listed for Test Cases 2e and 3e. This is due to the fact that the gains necessary for these maneuvers were already calculated in Test Cases 2c, 2d, 3c, and 3d. To perform Test Case 2e, a trajectory following controller should be implemented using the gains from Test Case 2d during spin-up and spin-down, while a disturbance rejection controller should be implemented using the gains from Test Case 2c during the steady state spin. In the same way, the gains from Test Case 3d should be used in a trajectory following controller during the spin-up and spin-down of Test Case 3e, while the gains from Test Case 3c should be used in a disturbance rejection controller during the steady state spin.

A.5.4 Spin-up

Input trajectories are necessary to dictate the spin-up and spin-down processes. While several approaches have been explored for Test Case 2e, no trajectory has been calculated for Test Case 3e. Three initial approaches to performing spin-up case 2e were explored by specifying a magnet current profile and determining the necessary reaction wheel profiles to perform spin-up.

The first approach was to turn on the magnets to the current necessary to hold the vehicles in place during steady state spin. A reaction wheel profile was then determined to rotate the vehicles to align for steady state. The current necessary for this maneuver was calculated by solving the following force equation for the magnetic moment $\mu = \mu_A = \mu_B$:

$$F_{EM,rad} = \frac{-3}{4\pi} \frac{\mu_0 \mu_A \mu_B}{(2r)^4} = m \dot{\theta}^2 r \quad \text{Equation A.5-13}$$

where $\mu_0 = 4\pi e^{-7}$, r is the 1 meter distance between vehicles, m is the mass of each vehicle at 20 kg, and $\dot{\theta}$ is the rotation rate of the array, set to 1 rpm. The value for μ was then plugged into the equation:

$$\mu = niA \quad \text{Equation A.5-14}$$

where n , the number of wraps in the coil, is 100 and A is the area of the coil, using 0.83 meters for the diameter. The steady state current necessary using these values was found to be 44.7 amps.

To find the torque profile, the following equations of motion were used:

$$m r \ddot{\theta} = F_{EM,TAN} - 2 \dot{\theta} \dot{r} m = \frac{3}{4\pi} \frac{\mu_0 \mu_A \mu_B}{r^4} (\sin \theta_B \cos \theta_A + \sin \theta_A \cos \theta_B) - 2 \dot{\theta} \dot{r} m \quad \text{Equation A.5-15}$$

$$m \dot{r} = F_{EM,RAD} + m \dot{\theta}^2 r = -\frac{3}{4\pi} \frac{\mu_0 \mu_A \mu_B}{r^4} (2 \cos \theta_A \cos \theta_B - \sin \theta_B \sin \theta_A) + m \dot{\theta}^2 r \quad \text{Equation A.5-16}$$

They were discretized to the form:

$$\ddot{\theta}_0 = \frac{1}{n} \frac{3}{4\pi} \frac{\mu_0 \mu_A \mu_B}{r_0^5} (\sin \theta_{B,0} \cos \theta_{A,0} + \sin \theta_{A,0} \cos \theta_{B,0}) - \frac{2 \dot{\theta}_0 \dot{r}_0}{r_0} \quad \text{Equation A.5-17}$$

$$\dot{r}_0 = -\frac{1}{n} \frac{3}{4\pi} \frac{\mu_0 \mu_A \mu_B}{r_0^4} (2 \cos \theta_{A,0} \cos \theta_{B,0} - \sin \theta_{B,0} \sin \theta_{A,0}) + \dot{\theta}_0^2 r_0 \quad \text{Equation A.5-18}$$

The initial conditions used to find the torque profile were:

- $\theta_{A,0} = \theta_A = 0$, from keeping the coordinate system fixed on vehicle A,
- $\theta_{B,0} = 90^\circ$, starting the magnet for vehicle B perpendicular to the magnet of vehicle A,
- $r_0 = r = 1\text{m}$, keeping the radius between vehicles constant,
- $\dot{\theta}_0 = \theta_0 = 0$
- $\dot{r} = \dot{r} = 0$.

The final conditions were:

- $\theta_{B,final} = 0^\circ$
- $\dot{\theta}_{final} = \frac{2\pi}{60} \text{rad/s}$

The following process is then iterated to find the torque profile:

$$\dot{\theta}_1 = \dot{\theta}_0 + \ddot{\theta}_0 dt \quad \text{Equation A.5-19}$$

$$F_{RAD,1} = \dot{\theta}_1^2 r_1 m \quad \text{Equation A.5-20}$$

$$\theta_{B,1} = \cos^{-1} \left(\frac{-F_{RAD,1} (2r)^4}{k_1} \right) \quad \text{Equation A.5-21}$$

$$\dot{\theta}_{B,1} = \frac{(\theta_{B,1} - \theta_{B,0})}{dt} \quad \text{Equation A.5-22}$$

$$F_{TAN,1} = \frac{k_1}{(2r)^4} (\sin \theta_{B,1} \cos \theta_A + \sin \theta_A \cos \theta_{B,1}) \quad \text{Equation A.5-23}$$

$$\ddot{\theta} = \frac{F_{TAN,1}}{mr} \quad \text{Equation A.5-24}$$

where $k = -\frac{3\mu_0\mu_A\mu_B}{4\pi}$, a constant for this method.

The torques on the electromagnets are calculated from the following equations:

$$\tau_{EM,zA} = \frac{k}{(2r)^3} (\cos(\theta_A) \sin(\theta_B) + 2 \sin(\theta_A) \cos(\theta_B)) \quad \text{Equation A.5-25}$$

$$\tau_{EM,zB} = \frac{k}{(2r)^3} (2 \cos(\theta_A) \sin(\theta_B) + \sin(\theta_A) \cos(\theta_B)) \quad \text{Equation A.5-26}$$

The torques on the reaction wheels are calculated from the following equations:

$$\tau_{RW,A} = -(mr^2 + I)\ddot{\theta} + \tau_{EM,xA} \quad \text{Equation A.5-27}$$

$$\tau_{RW,B} = -(mr^2 + I)\ddot{\theta} + I\ddot{\theta}_B + \tau_{EM,xB} \quad \text{Equation A.5-28}$$

The profiles are shown in Figure A.5-C and Figure A.5-D:

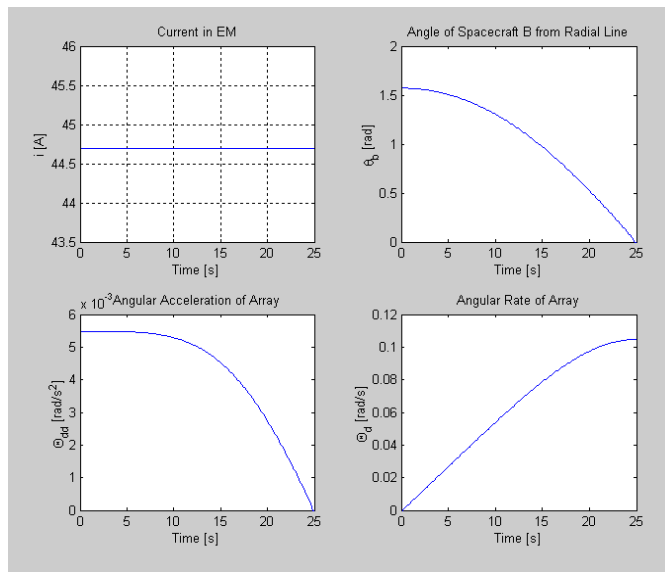


Figure A.5-C: EM and Angular Profiles for Constant EM Spin-up

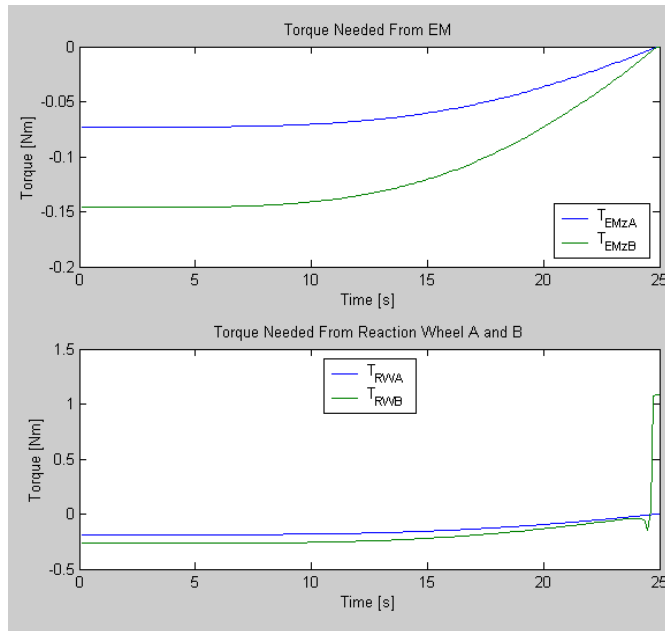


Figure A.5-D: Torque Profiles for Constant EM Spin-up

As shown in the graphs, this spin-up approach takes 25 seconds. The spike towards the end of the torque profile for reaction wheel B is due to a numerical error from a differentiation and does not reflect an actual physical occurrence. To test that this is true, the time step was changed and examined. The spike remained the same number of time steps from the end, indicating there was a numerical problem, not a physical problem.

To slow down spin-up, a second approach was explored. A ramp input was chosen for the electromagnet. The code written allows variable lengths for the ramp. For this case, a ramp time of 70 seconds was chosen to bring the electromagnet currents from 0 amps to

the steady state value 44.7 amps. This whole approach takes 85 seconds to complete, as shown in Figure A.5-E and Figure A.5-F.

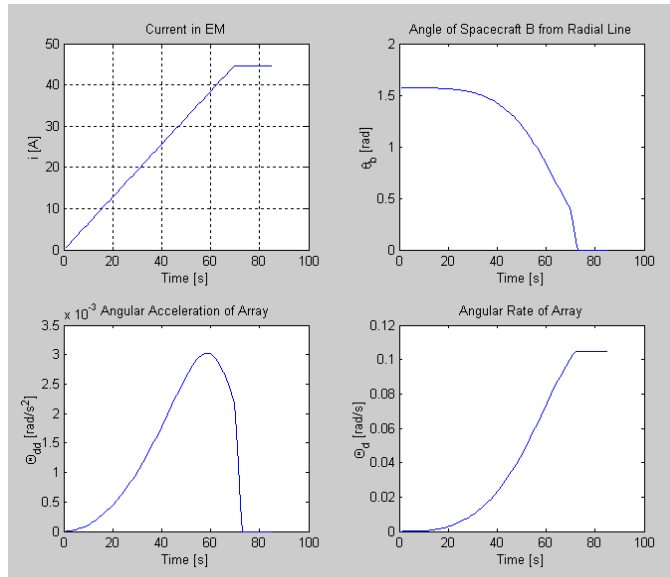


Figure A.5-E: EM and Angular Profiles for Ramped EM Spin-up

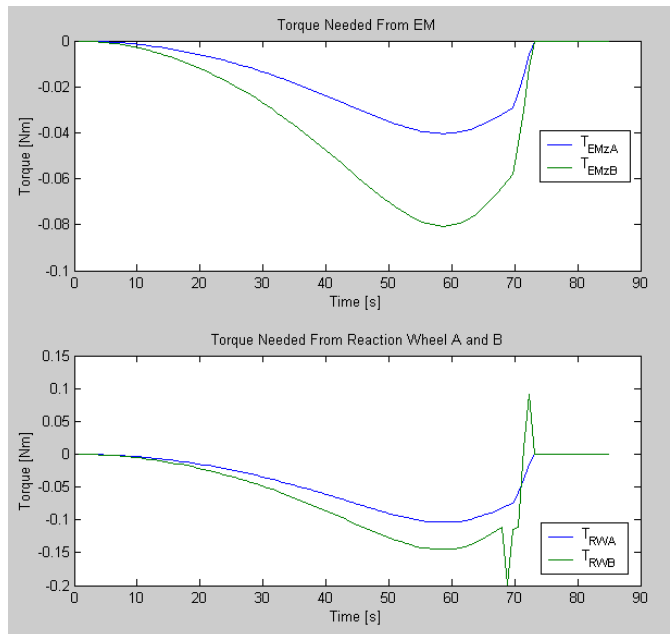


Figure A.5-F: Torque Profiles for Constant EM Spin-up

Once again, a numerical error caused the spike in reaction wheel B. The final approach explores a quicker spin-up profile by ramping the current in the electromagnets to twice the amount needed for steady state spin, and then ramping back down to the steady state current. The code for this case also allows variable ramp times. In the following graphs (Figure A.5-G and Figure A.5-H), the electromagnetic current is ramped up to twice the

steady state value in one second, held at that value for another 8 seconds, and then ramped down to the steady state value in another second.

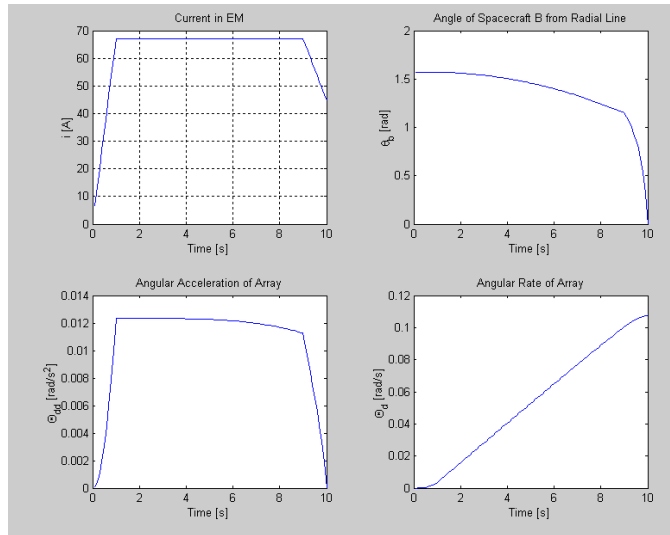


Figure A.5-G: EM and Angular Profiles for Double Ramped Approach

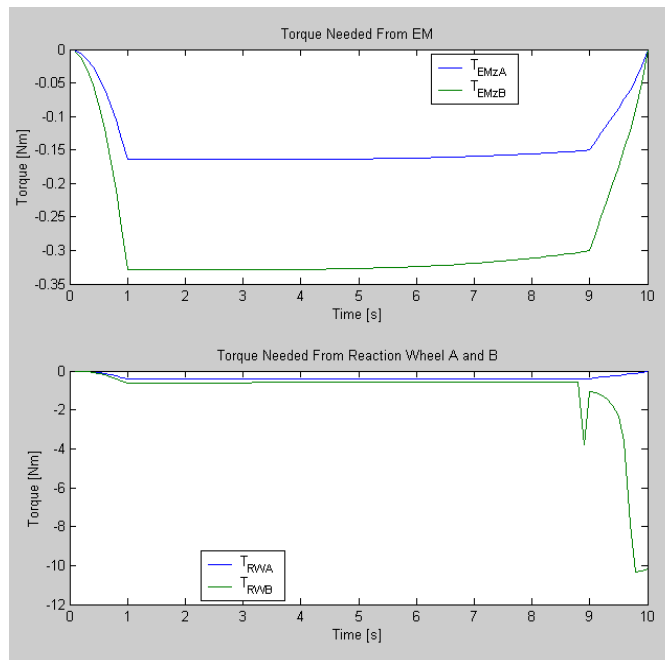


Figure A.5-H: Torque Profiles for the Double Ramped Approach

All three options present feasible electromagnet and reaction wheel profiles (with the exception of the numerical errors). Depending on the time constraints of spin-up and torque limits, one of these spin-up profiles could be chosen. However, examining the profiles for the angle of spacecraft B shows that the vehicle would quickly rotate towards a 90-degree turn and need to abruptly stop. This would require a lot of effort from the torque wheels to prevent overshoot in the turns. For this reason, another approach to

spin-up was explored using a pre-determined angular profile for vehicle B to determine the required electromagnet and reaction wheel profiles. In this approach, a profile for the angle of vehicle B (Figure A.5-I) is modeled as a section of a cosine wave, so the angle slowly approaches its end value. Differentiating this, an initial and final acceleration are specified, despite the fact that the initial and final angular velocities are zero.

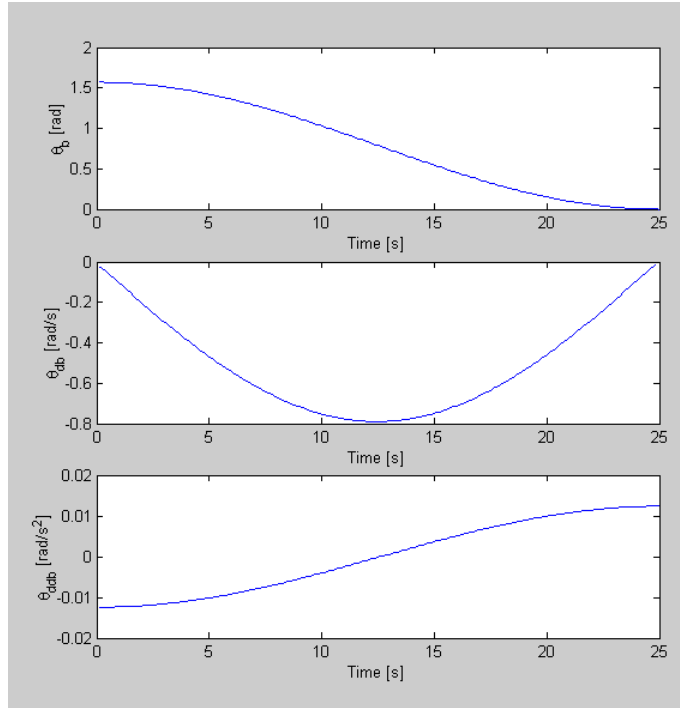


Figure A.5-I: Profiles for Spacecraft B

The initial acceleration will be created when the electromagnets are turned on. The final acceleration can be counteracted with the reaction wheels. It seems more feasible to counteract this acceleration with the reaction wheels than to counteract the increasing rotational velocity of the spacecraft from the first approach due to the fact that the velocity is approaching zero in the second case. Electromagnet and reaction wheel profiles have not been determined due to an error in the code. However, the approach to calculate them is described in the following equations.

The same initial conditions will be used for this approach. The angle of spacecraft B is specified by the following equation:

$$\theta_B(t) = \frac{\pi}{4} \cos\left(\frac{\pi}{t_f} t\right) + \frac{\pi}{4} \quad \text{Equation A.5-29}$$

F_{Rad1} is calculated using equations A.5-19 and A.5-20.

Then, the magnetic moments can be calculated.

$$\mu_{A,1}\mu_{B,1} = -\frac{F_{Rad,1}}{k_1(2\cos(\theta_A)\cos(\theta_{B,1}) + \sin(\theta_{B,1})\sin(\theta_A))} \quad \text{Equation A.5-30}$$

where $k_1 = \frac{3}{4\pi} \frac{\mu_0}{(2r)^4}$.

Then use

$$F_{Tan,1} = k_1\mu_{A,1}\mu_{B,1}(\sin(\theta_{B,1})\cos(\theta_A) + \sin(\theta_A)\cos(\theta_{B,1})) \quad \text{Equation A.5-31}$$

$$\ddot{\theta}_1 = \frac{F_{Tan,1}}{mr} \quad \text{Equation A.5-32}$$

along with Equations A.5-25 through A.5-28 to determine the reaction wheel profiles. The electromagnet current profiles can be calculated using Equations A.5-14 and A.5-30.

A.6 Interfacing

The main interfacing of the control team is with avionics, due to the fact that the controller will be located on the avionics computer. Preliminary discussions regarding the size and amount of the computations done by the controller helped decide what processor the avionics team chose.

Interfacing with metrology is necessary to determine the accuracy of the metrology sensing. Also, the interfacing determines which inputs the control team needs from metrology, and which inputs the metrology team is capable of providing. This also includes the communications team, who decides how this information is transmitted. The final decision for this interfacing includes a Primary Vehicle Array (PVA) that consists of the data from the metrology sensors, and a MSA, which consists of the state information to be inputted into the controller. Each vehicle will send its PVA to the other vehicles. The three PVAs can then be compiled by each vehicle into an MSA, which will be sent to the controller.

A.7 Coding Controllers in C

The next step in creating a controller was to code it into C. An advantage to using an LQR controller was the fact that all we needed to do was multiply the states by the gains, a simple matrix multiplication, to generate control output values.

For Test Case 1 our states are angle and angular rate. For the one vehicle case, however, we could only sense angular rate. Therefore to solve for the angle we integrated our angular rate over time. This was easily handled in the code. For Test Case 1b, we also had to add in a desired state and have this state change over time so that the vehicle would perform a preprogrammed maneuver. Since the controller is a Linear Quadratic Regulator it is constantly trying to keep a state at its nominal value. To make the vehicle move then one must “trick” the vehicle into thinking it is not at its nominal value and

wait for the vehicle to correct to the new nominal value. To accomplish this we simply subtracted the desired state from the input we received. For example, say the nominal angle value was zero. If you wanted to move the vehicle 30 degrees you would subtract 30 degrees from the input. This makes the vehicle think it's at -30 degrees thus the controller works to bring it back to the nominal.

The code for Test Case 2 is pretty straightforward. It runs off the same basic framework stated above. It reads the variables in to a state array, multiplies this array by the gains matrix, and writes the results into an output commands array. Trajectory following is handled just like in Test Case 1b, where the vehicle is tricked into thinking that it is not at the nominal state.

A.8 Controller Concerns and Mitigations

The control team has several concerns that have arisen during the design process. These include near field effects, the time constant of the electromagnets, and coding of the controllers.

The first concern arises because the system models were made using equations that are valid for the far field approximation of the electromagnet effects. The far field assumption is determined by the size of the electromagnets and their separation distances. If the electromagnets move closer into the near field, the model becomes less accurate.

The time constant of the electromagnet determines how quickly the current in the electromagnet and therefore the field produced by the electromagnet can be changed. The time constant required by the control team to successfully control the electromagnet is determined by the rotation rate of the system. If the time constant of the electromagnet proves to be slower than what is needed to control effectively, the rotation rate of the system must be slowed. The electromagnetic field must be able to be changed faster than the controller requires a change to perform maneuvers.

A.9 Optimal Gains

A.9.1 Test Case 1

$$R_{xx} = \begin{bmatrix} 10^{-5} & 0 \\ 0 & 1 \end{bmatrix} \quad R_{uu} = \frac{1}{4}$$

Figure A.9-A: Test case 1a weightings

Table A.9-1: Gains for Test Case 1a, I = 0.9 kg*m²

θ	$\dot{\theta}$	
0.0063	2.003	τ_{RW}

Table A.9-2: Gains for Test Case 1a, I = 1 kg*m2

θ	$\dot{\theta}$	
0.0063	2.003	τ_{RW}

$$R_{xx} = \begin{bmatrix} 1 & 0 \\ 0 & 10^{-4} \end{bmatrix} \quad R_{uu} = \frac{1}{4}$$

Figure A.9-B: Test Case 1b Weightings**Table A.9-3: Gains for Test Case 1b, I = 0.9 kg*m2**

θ	$\dot{\theta}$	
2.000	1.898	τ_{RW}

Table A.9-4: Gains for Test Case 1b, I = 1 kg*m2

θ	$\dot{\theta}$	
2.000	2.001	τ_{RW}

A.9.2 Test Case 2

Table A.9-5: Constants used to calculate gains for Test Case 2

$\mu_{B,1}$	$\mu_{B,2}$	m_A	$I_A = I_B$	r
1767.1 A*m ²	176.71 A*m ²	15 kg	1 kg*m ²	2 meters

$$R_{xx} = \begin{bmatrix} \mathbf{0} & \mathbf{0} \\ \hline 1 & 0 & 0 \\ \mathbf{0} & 0 & 1 & 0 \\ 0 & 0 & 0 & 1 \end{bmatrix} \quad R_{uu} = \begin{bmatrix} 0.25 & 0 & 0 \\ 0 & 0.25 & 0 \\ 0 & 0 & 0.125 \end{bmatrix}$$

Figure A.9-C: Test Case 2a weightings

Table A.9-6: Gains for Test Case 2a

x_A	y_A	θ_A	\dot{x}_A	\dot{y}_A	$\dot{\theta}_A$	
-0.0063	0.0004	-0.0000	-23.9293	1.9237	-0.0000	μ_{A1}
0.0004	0.0063	-0.0000	1.9237	33.7807	-0.0003	μ_{A2}
0.0000	0.0000	0.0089	0.0001	0.0060	2.8316	$\tau_{RW,A}$

$$R_{xx} = \left[\begin{array}{ccc|c} 1 & 0 & 0 & \mathbf{0} \\ 0 & 1 & 0 & \mathbf{0} \\ 0 & 0 & 1 & \mathbf{0} \\ \hline \mathbf{0} & \mathbf{0} & \mathbf{0} & \mathbf{0} \end{array} \right] \quad R_{uu} = \begin{bmatrix} 0.25 & 0 & 0 \\ 0 & 0.25 & 0 \\ 0 & 0 & 0.125 \end{bmatrix}$$

Figure A.9-D: Test Case 2b weightings

Table A.9-7: Gains for Test Case 2b

x_A	y_A	θ_A	\dot{x}_A	\dot{y}_A	$\dot{\theta}_A$	
-1.9956	0.1330	-0.0000	-424.0485	34.1238	-0.0000	μ_{A1}
0.1330	1.9956	-0.0002	34.1239	599.6666	-0.0002	μ_{A2}
0.0000	0.0004	2.8284	0.0023	0.1063	2.3784	$\tau_{RW,A}$

$$R_{xx} = \left[\begin{array}{c|cccc} \mathbf{0} & & & & \\ \hline & 1 & 0 & 0 & 0 \\ \mathbf{0} & 0 & 1 & 0 & 0 \\ & 0 & 0 & 1 & 0 \\ & 0 & 0 & 0 & 1 \end{array} \right] \quad R_{uu} = \begin{bmatrix} 0.25 & 0 & 0 & 0 \\ 0 & 0.25 & 0 & 0 \\ 0 & 0 & 0.125 & 0 \\ 0 & 0 & 0 & 0.125 \end{bmatrix}$$

Figure A.9-E: Test Case 2c weightings

Table A.9-8: Gains for Test Case 2c

x_A	y_A	θ_A	θ_B	\dot{x}_A	\dot{y}_A	$\dot{\theta}_A$	$\dot{\theta}_B$	
- 0.0063	0.0004	-0.0000	-0.0000	-23.9293	1.9237	-0.0000	-0.0000	μ_{A1}
0.0004	0.0063	-0.0000	-0.0000	1.9237	33.7807	-0.0003	-0.0001	μ_{A2}
0.0000	0.0000	0.0089	-0.0000	0.0001	0.0060	2.8316	-0.0000	$\tau_{RW,A}$
- 0.0000	0.0000	-0.0000	0.0089	-0.0003	0.0030	-0.0000	2.8316	$\tau_{RW,B}$

$$R_{xx} = \left[\begin{array}{cccc|c} 1 & 0 & 0 & 0 & \mathbf{0} \\ 0 & 1 & 0 & 0 & \\ 0 & 0 & 1 & 0 & \\ 0 & 0 & 0 & 1 & \\ \hline \mathbf{0} & & & & \mathbf{0} \end{array} \right] \quad R_{uu} = \begin{bmatrix} 0.25 & 0 & 0 & 0 \\ 0 & 0.25 & 0 & 0 \\ 0 & 0 & 0.125 & 0 \\ 0 & 0 & 0 & 0.125 \end{bmatrix}$$

Figure A.9-F: Test Case 2d weightings

Table A.9-9: Gains for Test Case 2d

x_A	y_A	θ_A	θ_B	\dot{x}_A	\dot{y}_A	$\dot{\theta}_A$	$\dot{\theta}_B$	
-1.9956	0.1330	-0.0000	-0.0000	-424.0485	34.1238	-0.0000	-0.0000	μ_{A1}
0.1330	1.9956	-0.0002	-0.0001	34.1238	599.6666	-0.0002	-0.0001	μ_{A2}
0.0000	0.0004	2.8284	-0.0000	0.0023	0.1063	2.3784	-0.0000	$\tau_{RW,A}$
-0.0000	0.0002	-0.0000	2.8284	-0.0045	0.0536	-0.0000	2.3784	$\tau_{RW,B}$

A.9.3 Test Case 3

Table A.9-10: Constants used to calculate gains for Test Case 2

$\mu_{B,1}$	$\mu_{B,2}$	$m_A = m_B = m_B$	$I_A = I_B = I_C$	$r_{AB} = r_{BC}$
1767.1 A*m ²	176.71 A*m ²	15 kg	1 kg*m ²	2 meters

$$R_{xx} = \left[\begin{array}{c|cccccc} \mathbf{0} & & & & & \\ \hline & \mathbf{0} & & & & \\ & 1 & 0 & 0 & 0 & 0 \\ & 0 & 1 & 0 & 0 & 0 \\ \mathbf{0} & 0 & 0 & 1 & 0 & 0 \\ & 0 & 0 & 0 & 1 & 0 \\ & 0 & 0 & 0 & 0 & 1 \\ & 0 & 0 & 0 & 0 & 0 \\ & 0 & 0 & 0 & 0 & 1 \end{array} \right]$$

$$R_{uu} = \begin{bmatrix} 0.25 & 0 & 0 & 0 & 0 & 0 \\ 0 & 0.25 & 0 & 0 & 0 & 0 \\ 0 & 0 & 0.25 & 0 & 0 & 0 \\ 0 & 0 & 0 & 0.25 & 0 & 0 \\ 0 & 0 & 0 & 0 & 0.125 & 0 \\ 0 & 0 & 0 & 0 & 0 & 0.125 \end{bmatrix}$$

Figure A.9-G: Test Case 3a weightings

Table A.9-11: Gains for Test Case 3a

x_A	x_B	y_A	y_B	θ_A	θ_B	\dot{x}_A	\dot{x}_B	\dot{y}_A	\dot{y}_B	$\dot{\theta}_A$	$\dot{\theta}_B$	
-0.0063	0	0.0004	0	0	0	-23.9293	0	1.9237	0	0	0	μ_{A1}
0.0004	0	0.0063	0	0	0	1.9237	0	33.7807	0	0.0003	0	μ_{A2}
0	-0.0063	0	0.0004	0	0	0	-23.9293	0	1.9237	0	0	μ_{B1}
0	0.0004	0	0.0063	0	0	0	1.9237	0	33.7807	0	-0.0003	μ_{B2}
0	0	0	0	0.0089	0	0.0001	0	0.006	0	2.8318	0	$\tau_{RW,A}$
0	0	0	0	0	0.0089	0	0.0001	0	0.006	0	2.8318	$\tau_{RW,B}$

$$R_{xx} = \left[\begin{array}{c|cccccc} 1 & 0 & 0 & 0 & 0 & 0 \\ 0 & 1 & 0 & 0 & 0 & 0 \\ 0 & 0 & 1 & 0 & 0 & 0 \\ 0 & 0 & 0 & 1 & 0 & 0 \\ 0 & 0 & 0 & 0 & 1 & 0 \\ 0 & 0 & 0 & 0 & 0 & 1 \\ \hline \mathbf{0} & & & & & \mathbf{0} \end{array} \right]$$

$$R_{uu} = \begin{bmatrix} 0.25 & 0 & 0 & 0 & 0 & 0 \\ 0 & 0.25 & 0 & 0 & 0 & 0 \\ 0 & 0 & 0.25 & 0 & 0 & 0 \\ 0 & 0 & 0 & 0.25 & 0 & 0 \\ 0 & 0 & 0 & 0 & 0.125 & 0 \\ 0 & 0 & 0 & 0 & 0 & 0.125 \end{bmatrix}$$

Figure A.9-H: Test Case 3b weightings

$$R_{xx} = \left[\begin{array}{cccccc|c} 1 & 0 & 0 & 0 & 0 & 0 & 0 \\ 0 & 1 & 0 & 0 & 0 & 0 & 0 \\ 0 & 0 & 1 & 0 & 0 & 0 & 0 \\ 0 & 0 & 0 & 1 & 0 & 0 & 0 \\ 0 & 0 & 0 & 0 & 1 & 0 & 0 \\ 0 & 0 & 0 & 0 & 0 & 1 & 0 \\ 0 & 0 & 0 & 0 & 0 & 0 & 1 \\ \hline & & & & & & 0 \end{array} \right]$$

$$R_{uu} = \left[\begin{array}{cccccc} 0.25 & 0 & 0 & 0 & 0 & 0 \\ 0 & 0.25 & 0 & 0 & 0 & 0 \\ 0 & 0 & 0.25 & 0 & 0 & 0 \\ 0 & 0 & 0 & 0.25 & 0 & 0 \\ 0 & 0 & 0 & 0 & 0.125 & 0 \\ 0 & 0 & 0 & 0 & 0 & 0.125 \\ 0 & 0 & 0 & 0 & 0 & 0.125 \end{array} \right]$$

Figure A.9-J: Test Case 3d weightings

Table A.9-14: Gains for Test Case 3d

x_A	x_B	y_A	y_B	θ_A	θ_B	θ_C	\dot{x}_A	\dot{x}_B	\dot{y}_A	\dot{y}_B	$\dot{\theta}_A$	$\dot{\theta}_B$	$\dot{\theta}_C$	
-1.9956	0	0.133	0	0	0	0	-424.049	0	34.1238	0	0	0	0	μ_{A1}
0.133	0	1.9956	0	-0.0002	0.0001	0	34.1238	0	599.6666	0	-0.0002	-0.0001	0	μ_{A2}
0	-1.9956	0	0.133	0	0	0	0	-424.049	0	34.1238	0	0	0	μ_{B1}
0	0.133	0	1.9956	0	0.0001	-0.0002	0	34.1238	0	599.667	0	-0.0001	0.0002	μ_{B2}
0	0	0.0004	0	2.8284	0	0	0.0023	0	0.1063	0	2.4426	0	0	$\tau_{RW,A}$
0	0	0.0002	0.0002	0	2.8284	0	-0.0045	-0.0045	0.0536	0.0536	0	2.4426	0	$\tau_{RW,B}$
0	0	0	0.0004	0	0	2.8284	0	0.0023	0	0.1063	0	0	2.4426	$\tau_{RW,C}$

Spin-up

Table A.9-15: Constants used to calculate gains for spin-up

R	$\dot{i} = \ddot{i}$	m	Ω	n	d_{coil}	$i_{\text{ss, EM}}$	$\theta_{A,0} = \theta_A$	$\theta_{B,0}$	$\theta_{B,\text{final}}$	I
1 meter	0	20 kg	1 rpm	100 wraps	0.83 m	44.7 Amps	0	90°	0°	1 kg*m ²